Elevated Glutamatergic Compounds in Pregenual Anterior Cingulate in Pediatric Autism Spectrum Disorder Demonstrated by ^{1}H MRS and ^{1}H MRSI

Anthony Bejjani[3], Joseph O'Neill[1]*, John A. Kim[2], Andrew J. Frew[3], Victor W. Yee[1], Ronald Ly[1], Christina Kitchen[4], Noriko Salamon[5], James T. McCracken[1,6], Arthur W. Toga[2,6], Jeffry R. Alger[3,6], Jennifer G. Levitt[1]

1 Division of Child and Adolescent Psychiatry, Semel Institute for Neurosciences, David Geffen School of Medicine at UCLA, Los Angeles, California, United States of America, 2 Laboratory of Neuroimaging, Department of Neurology, David Geffen School of Medicine at UCLA, Los Angeles, California, United States of America, 3 Ahmanson-Lovelace Brain Mapping Center, Department of Neurology, David Geffen School of Medicine at UCLA, Los Angeles, California, United States of America, 4 Department of Biostatistics, David Geffen School of Medicine at UCLA, Los Angeles, California, United States of America, 5 Department of Radiological Sciences, David Geffen School of Medicine at UCLA, Los Angeles, California, United States of America, 6 Brain Research Institute, David Geffen School of Medicine at UCLA, Los Angeles, California, United States of America

Abstract

Recent research in autism spectrum disorder (ASD) has aroused interest in anterior cingulate cortex and in the neurometabolite glutamate. We report two studies of pregenual anterior cingulate cortex (pACC) in pediatric ASD. First, we acquired *in vivo* single-voxel proton magnetic resonance spectroscopy (^{1}H MRS) in 8 children with ASD and 10 typically developing controls who were well matched for age, but with fewer males and higher IQ. In the ASD group in midline pACC, we found mean 17.7% elevation of glutamate + glutamine (Glx) ($p<0.05$) and 21.2% ($p<0.001$) decrement in creatine + phosphocreatine (Cr). We then performed a larger (26 subjects with ASD, 16 controls) follow-up study in samples now matched for age, gender, and IQ using proton magnetic resonance spectroscopic imaging (^{1}H MRSI). Higher spatial resolution enabled bilateral pACC acquisition. Significant effects were restricted to right pACC where Glx (9.5%, $p<0.05$), Cr (6.7%, $p<0.05$), and *N*-acetyl-aspartate + *N*-acetyl-aspartyl-glutamate (10.2%, $p<0.01$) in the ASD sample were *elevated* above control. These two independent studies suggest hyperglutamatergia and other neurometabolic abnormalities in pACC in ASD, with possible right-lateralization. The hyperglutamatergic state may reflect an imbalance of excitation over inhibition in the brain as proposed in recent neurodevelopmental models of ASD.

Introduction

Proposed abnormal glutamate (Glu) metabolism in autism spectrum disorder (ASD) [1–7] is supported by several lines of evidence. Epilepsy is common in ASD [8] and epileptic seizures are propagated by excitatory Glu. Elevated Glu and other excitatory amino acids have been reported in blood serum, plasma, and platelets in ASD [9–13]. Post-mortem neuropathology in ASD has found elevated mRNA or protein levels of glutamatergic transporters and neurotransmitter receptors [14]. And finally, ASD has been associated with single-nucleotide polymorphisms (SNPs) in glutamatergic genes, including those coding for transporters [15], metabotropic and ionotropic receptors [3,16,17], the enzyme glutamate decarboxylase [18], and the mitochondrial aspartate/glutamate carrier [19–26]. The last listed is also supported by neuropathology [27]. These various linkages give ample reason to ask if brain levels of Glu and related metabolites are disturbed in ASD and if such abnormalities have a

bearing on clinical presentation. Neuroimaging assays of regional levels of these compounds may help evaluate glutamatergic theories of ASD and inform potential therapies targeting Glu in specific brain structures.

Proton magnetic resonance spectroscopy (^{1}H MRS) is a neuroimaging technique that measures in vivo brain Glu safely and non-invasively in children. Thereby, "Glx", the combined signal for Glu and spectrally overlapping glutamine (Gln), is often more reliably assayed than Glu alone, especially at low field (<3 T). MRS investigations of autistic spectrum disorders have been numerous [28–52], but few have reported Glu or Glx [28,31,32,35,47,53]. All of these studies detected evidence of glutamatergic abnormalities except Friedman et al.[31,32], who examined very young (<5 years old) children with ASD. This suggests that further exploration of regional Glu and Glx in the brain in ASD is warranted.

One brain region frequently implicated in ASD, but where glutamatergic metabolites have been little explored [53], is the

Table 1. Experiment 1: Subject group characteristics.

group	gender	age, years	full-scale IQ	medication
ASD	7 male, 1 female	11.2±2.6 (7.8–15.9)	**90.0±11.5*** (74–105)	1 fluoxetine, *2* methylphenidate
Typically developing	5 male, 5 female	13.2±2.5 (7.4–16.5)	112.3±18.5 (83–137)	None

*$p<0.05$ vs. controls; values for age and IQ are group mean ± standard deviation (range).
doi:10.1371/journal.pone.0038786.t001

anterior cingulate cortex. Evidence from several investigative modalities points to involvement of the anterior cingulate in ASD, including neuropathology [54–57], structural MRI [58–62], fMRI [63–67], MRS [33,42,46,53], PET [68,69], SPECT [70], and EEG evoked potentials [71]. One hypothesis also relates anterior cingulate dysfunction to deficits in joint attention and social orienting in ASD [72]. This plentiful prior work gives reason to search for further abnormalities, perhaps involving the glutamatergic system, in anterior cingulate. Here, we report on two independent studies of glutamatergic neurometabolites in the anterior cingulate cortex in pediatric ASD; the first a pilot study, the second a larger follow-up investigation.

Within the cingulate gyrus, our investigations focused on the pregenual anterior cingulate cortex (pACC) subregion, one of the eight subregions in Vogt's definitive parcellation of the human cingulate cortex [73,74]. Most of the above-cited neuroimaging studies localized their acquisition or analysis volumes based on the older four-subregion or two-subregion cingulate models. As the eight-subregion model is most consistent with extant neuropathological, neuroimaging, and neurocognitive data, we anticipated that focusing on a subregion within this model would improve odds of detecting Glx effects and would permit more anatomically standardized statement of our results. Moreover, recent neuroimaging investigations, including multimodal MRS-fMRI and combined fMRI and genetic work, of autistic symptoms and autistic traits in healthy subjects have demonstrated focal effects within the pACC, raising the possibilities for finding MRS effects there as well [65,66,75,76].

Experiment 1

The first experiment was a pilot study targeting possible abnormalities in Glx in ASD in the pACC. The midline (left + right) pACC was sampled using single-voxel MRS.

Methods

Eight high-functioning subjects with ASD (1 female; mean ± SD age: 11.2±2.6 years, range: 7.8–15.9 years) and 10 typically developing control subjects (5 female; 13.2±2.5 years, 7.4–16.5 years) free of developmental or psychiatric disorder participated (Table 1). Seven subjects with ASD met criteria for autism and one subject met criteria for PDD-NOS according to the Autism Diagnostic Interview Revised (ADI-R) and the Autism Diagnostic Observation Schedule (ADOS) [77–78]. These standardized instruments were administered by study personnel trained to reliability by Dr. Catherine Lord's research group. Exclusionary criteria included the presence of major medical or neurologic illness, including epilepsy, and presence of a known genetic syndrome associated with autism such as Fragile X. Control subjects were recruited from local community schools. All subjects were screened for neurological, language, hearing or psychiatric disorders by K-SADS-PL interview with the parent [79]. Exclusion criteria for healthy controls included any lifetime

significant medical or Axis I mental disorder. The two subject samples did not differ significantly in age. One subject with ASD was on fluoxetine, two were on methylphenidate, and the remaining subjects were receiving no psychoactive medication at time of scan. No controls were undergoing neuropharmacologic treatment at time of MRS. Mean full-scale IQ (Wechsler Intelligence Scale for Children – WISC) [80] was 90.0±11.5 (74–105) for the sample with ASD and 112.3±18.5 (83–137) for the control sample, a significant difference (p<0.05, independent T-test of rank-transformed data). The study was approved by the UCLA Human Subjects Review Board and we obtained written, informed consent from all subjects or from the subjects' parents or guardians.

MRI and single-voxel ^{1}H MRS were acquired contemporaneously at 1.5 T on a GE Signa 5× system with a quadrature head coil. After sagittal scout, a whole-brain axial fast spin-echo MRI yielding proton density-weighted images and a coronal T1-weighted MRI (brain stem and forward) were acquired. These two MRI volumes were used to position single-voxel water-suppressed point-resolved spectroscopy (PRESS) ^{1}H MRS (GE PROBE, repetition time [TR] = 1500 ms, echo-time [TE] = 25 ms, number of excitations = 256) in midline pACC (Fig. 1) in order to assess potential group differences in local metabolite levels. Voxel position and volume (2.4–3.6 cc, 12–15 mm on a side) were varied to maximize gray-matter content. This procedure was applied identically for subjects with ASD and controls by operators blinded to subject diagnosis. The pACC was identified on MRI as the cingulate cortex directly rostral to the genu of the corpus callosum where the posterior wall of the MRS voxel was placed. Each scan was examined post-acquisition. When quality was low, the scan was repeated. Total session time was 1–1.5 hours. One subject with ASD was sedated with intravenous propofol during acquisition. Results for this subject did not differ markedly from those of the other subjects with ASD. In a separate MR session, a sagittal whole-brain volumetric acquisition was performed using a spoiled gradient recalled echo (SPGR) sequence (TR = 24 ms, TE = 9 ms, number of excitations = 2, in-plane resolution = 0.94×0.94 mm^2, partition thickness = 1.2 mm), yielding T1-weighted images used for MRI tissue-segmentation.

Operators were blinded to subject identity during MRS and MRI post-processing. MRS PROBE data were processed automatically with LCModel [81]. LCModel yielded absolute levels in Institutional Units (IU) scaled to water and accounting for variable voxel volume for five major metabolite peaks. The first peak represented the sum of the (very closely overlapping) signals for N-acetyl-aspartate (NAA) and N-acetyl-aspartyl-glutamate (NAAG); the sum is referred to as "total NAA", abbreviated "tNAA". The second peak, "Glx", was for the sum of glutamate and glutamine. The third was for the sum of creatine and phosphocreatine, together abbreviated "Cr". The fourth was for the sum of the choline-containing compounds phosphocholine, glycerophosphocholine, choline proper, and acetylcholine, together abbreviated "Cho". The final peak was for the sugar myo-inositol ("mI").

Figure 1. Axial-oblique spin-echo MRI of the brain at level of the basal ganglia showing position of midline pregenual anterior cingulate (pACC) proton magnetic resonance spectroscopy voxel (*white box*). Experiment 1.
doi:10.1371/journal.pone.0038786.g001

Table 2. Experiment 1: Voxel tissue content and proton magnetic resonance spectroscopy (^{1}H MRS) metabolite levels in midline pregenual anterior cingulate cortex (pACC) voxel.

	ASD		Healthy Control	
	mean ± SD	range	mean ± SD	range
Vol% GM	88.9±4.1	83.3–93.9	83.9±5.6	74.1–89.6
Vol% WM	6.4±2.2*	3.0–10.2	10.8±4.3	4.4–20.4
Vol% CSF	4.7±3.1	1.8–10.7	5.1±4.4	0.1–13.7
tNAA	7.4±1.6	4.6–9.7	7.5±1.1	6.4–9.5
Glx	17.0±1.4*	14.7–19.2	14.5±3.0	9.4–18.8
Cr	4.4±0.8*	2.8–5.4	5.6±0.7	4.7–6.7
Cho	1.1±0.2	0.8–1.4	1.2±0.3	0.9–1.9
mI	3.7±0.4	3.3–4.5	4.4±0.9	3.0–5.7

*$p<0.05$ vs. controls controls analysis-of-covariance covarying gender and vol% WM on rank-transformed (non-parametric) data, Bonferroni-corrected for multiple comparisons with a priori hypotheses.
SD = standard deviation, GM = gray matter, WM = white matter, CSF = cerebrospinal fluid.
tNAA = N-acetyl-aspartate + N-acetyl-aspartyl-glutamate, Glx = glutamate + glutamine, Cr = creatine + phosphocreatine, Cho = choline compounds, mI = myo-inositol.
doi:10.1371/journal.pone.0038786.t002

Numerous weaker resonances, in particular lipids and macromolecules, were included in the fit. Analyses were restricted to spectra with linewidth (full-width at half-maximum) ≤0.10 ppm and with signal-to-noise ratio ≥5 and to metabolite peaks that passed the widely applied standard LCModel automated quality control criterion SD ≤20%, supplemented by operator inspection. SPGR-derived T1-weighted MRI volumes were tissue-segmented into gray matter, white matter, and CSF whole-brain component volumes [82] then co-registered into the axial plane of the fast spin-echo MRI, which was already in register with the MRS voxels. A home-written software program in the Interactive Data Language (IDL; Research Systems Inc., Boulder, CO) then extracted volume% gray matter, white matter, and CSF in each MRS voxel. LCModel absolute metabolite levels were then corrected for volume% CSF. Metabolite levels were not corrected for T1- or T2-relaxation.

Given the small number of subjects, data were rank-transformed to provide for non-parametric statistical analyses. MRS voxel tissue composition (volume% gray matter, white matter, CSF) was compared between groups using independent T-test of rank-transformed data. CSF-corrected levels of each metabolite were compared between groups using analysis of covariance (ANCOVA) of rank-transformed data with subject gender as covariate. At sites where tissue composition differed significantly between groups, the relevant volume% variable(s) were added as covariates to ANCOVA. Criterion for statistical significance was $p<0.05$, Bonferroni-corrected for multiple comparisons with numbered a priori hypotheses. Effects were hypothesized on metabolites in the following order: 1. Glx, 2. tNAA, 3. Cr, 4. Cho, 5. mI.

Results and Discussion

MRS voxel volume% ranged 74.1–93.9% for gray matter, 3.0–20.4% for white matter, and 0.1–13.7% for CSF (Table 2). Volume% white matter in pACC was significantly lower in subjects with ASD (6.4±2.2%) than in controls (10.8±4.2%; $p<0.05$); otherwise tissue composition did not differ significantly between groups.

Fig. 2 shows sample LCModel-fitted ^{1}H MR spectra for a subject from the sample with ASD and a control subject. To the naked eye the Glx peak is larger in the subject with ASD than in the control. High Glx levels were also seen in most of the other subjects with ASD (Fig. 3). Table 2 lists group-mean CSF-corrected LCModel-derived metabolite values in pACC. For subjects with ASD vs. typically-developing controls, ANCOVA covarying for gender and volume% white matter found significantly higher Glx (17.7%; $p<0.05$) and significantly lower Cr (21.2%; $p<0.05$; Fig. 3). No significant effects were found for any other metabolite. Glx was above the control mean for 7 of 8 subjects with ASD. Upon removing subjects on medication, the single-voxel MRS Glx elevation in pACC was still significant (23.2%, $p<0.05$).

This pilot single-voxel MRS investigation of glutamatergic metabolites in pACC yielded two findings: 1) Glx was consistently higher in subjects with ASD than in typically-developing control subjects and 2) Cr was lower in subjects with ASD than in controls. These findings suggest that abnormal physiology of the anterior cingulate in ASD may include disturbances in Glu or Cr neurometabolism and signal the pACC as one locus of abnormality within the cingulate gyrus.

The first finding was elevated Glx (= Glu + Gln) in the pACC. This supports the notion of glutamatergic disturbances in ASD [1–7] and favors proposals of hyper- as opposed to hypoglutamatergia, at least in the pACC. Glu is normally the larger component of the Glx signal and is present in tissue in both neurotransmitter and metabolic pools, which cannot be distinguished by in vivo ^{1}H MRS [83]. Mechanisms that might increase the combined Glu + Gln = Glx concentration include greater pre-synaptic vesicular release of Glu and co-localized NAAG [84], faster breakdown of NAAG into NAA and Glu [85], and net production rather than consumption of Glu by the Krebs Cycle in neurons and astrocytes [86], slower conversion of Gln to GABA [87], and net production rather than consumption of Gln by the Krebs Cycle. Moreover, Gln is exported from the astrocyte by the SNAT3 [88] neutral amino acid membrane transporter, crosses extracellular fluid, and
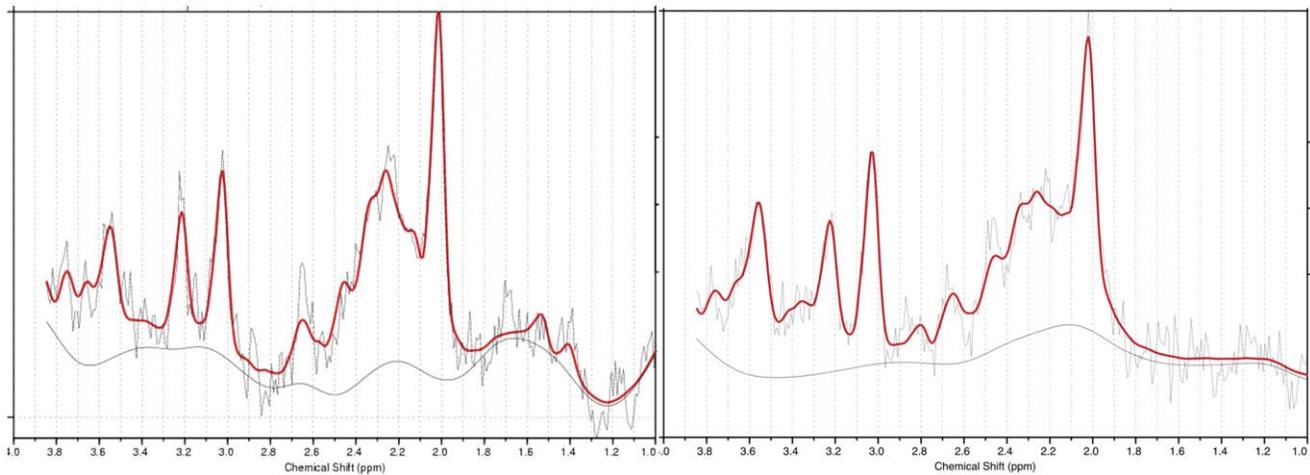
Figure 2. Raw (*light gray*), fit (*heavy solid red*), and baseline (*solid gray*) LCModel (Provencher 2001) output spectra for proton magnetic resonance spectroscopy voxels placed in midline pregenual anterior cingulate (pACC) in study subject with *ASD* (*left*) and control subject (*right*). Note larger Glx peak (2.0–2.5 ppm) in subject with *ASD*. Seven of 8 subjects with *ASD* exhibited Glx levels above the control mean (Fig. 3). Experiment 1.
doi:10.1371/journal.pone.0038786.g002

is taken into the neuron by the SNAT1 transporter [89]. Slowing of this Gln transport resulting in longer residence times in the Glu-Gln Cycle [86,90,91] would also lead to higher effective Glx levels. Consequences of chronic excess Glx could include abnormal development, ongoing excitotoxic cell damage (particularly in the case of Glu in the neurotransmitter pool), and inefficient utilization of cell energy.

The second finding was diminished Cr in the pACC. Creatine and phosphocreatine are principal reactants in the cellular buffer for maintenance and rapid mobilization of ATP energy [92–94]. This Cr deficit, along with the above Glx excess and previously demonstrated [18]FDG-PET abnormalities in ASD [95], may reflect locally aberrant cell-energy metabolism.

Results will be compared, in conjunction with those of Experiment 2, to previous MRS investigations in a combined discussion below.

This pilot investigation had a small number of subjects. Subjects with ASD were compared to a control group that was not well matched for gender or IQ. Three subjects with ASD were receiving regular psychotropic medication and one underwent sedation during the MRS scan; no controls underwent such pharmacologic treatments. Left and right pACC were sampled together in a single MRS voxel; that voxel contained, on average more white matter in subjects with ASD than in controls (although vol% white matter was under 10% in most subjects and was covaried for statistically). Despite these limitations, Experiment 1 gives a strong indication (7 of 8 subjects) of above-normal glutamatergic compounds in the pACC in ASD. Experiment 2 attempted to address some of the above limitations.

Experiment 2

The second experiment was a larger study that again targeted Glx in ASD in the pACC. This time, the higher spatial resolution of the proton magnetic resonance spectroscopic imaging (^{1}H MRSI) technique allowed us to examine left and right pACC
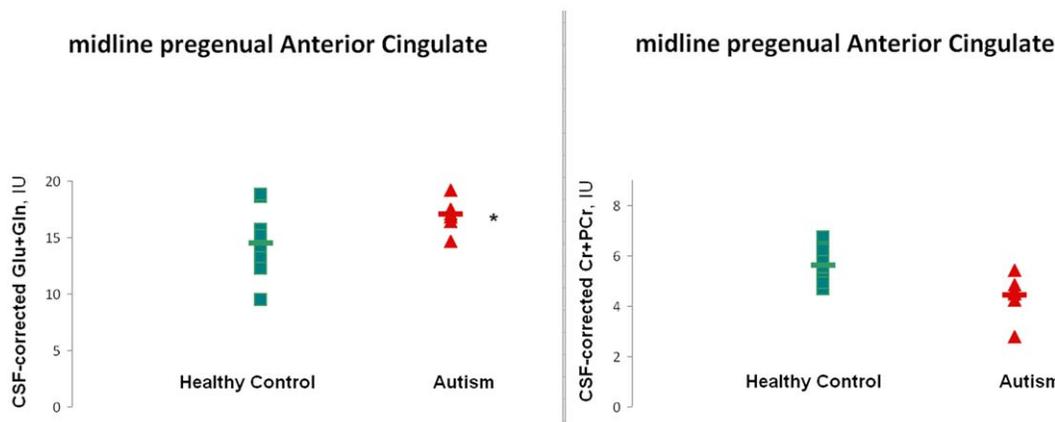
Figure 3. LCModel-derived absolute metabolite levels in Institutional Units (IU) corrected for voxel CSF-content for subjects with *ASD* (*red triangles*) and healthy controls (*green squares*). *Horizontal bars* denote group means. Values are shown for glutamate + glutamine ("Glx"; *left*) and creatine + phosphocreatine (*right*) in pACC. Note elevated Glx and depressed Cr + PCr in subjects with *ASD*. *$p < .05$, **$p < .01$ (independent T-test following ANCOVA of rank-transformed, therefore non-parametric data.) Experiment 1.
doi:10.1371/journal.pone.0038786.g003

separately, and therefore permitted us to investigate any lateralized effects on glutamatergic metabolites in this region. MRSI furthermore enabled us to investigate the possibility that results of Experiment 1 were influenced by white-matter intrusion into the MRS voxel by additionally obtaining metabolite levels in the prefrontal white-matter regions laterally adjacent to left and right pACC. Subjects with ASD were now compared to typically developing control subjects who were matched for age, gender, and IQ. Based on the results of Experiment 1, we hypothesized elevated Glx and diminished Cr in ASD in pACC, without any preference for the left or right hemisphere.

Methods

Twenty-six high-functioning subjects with ASD (7 female; mean ± SD age: 10.2±3.3 years, range: 6.1–17.5 years) and 16 typically developing control subjects (5 female; 11.8±3.0 years, 7.3–16.6 years) participated (Table 3). No subject in Experiment 2 was also a subject in Experiment 1. As in Experiment 1, exclusionary criteria included the presence of major medical or neurologic illness, including epilepsy, and presence of a known genetic syndrome associated with autism such as Fragile X. Subjects with ASD were recruited from the Autism Genetic Research Exchange (AGRE) and were included only if they had met criteria for ASD based upon the Autism Diagnostic Interview-Revised (ADI-R) [77] interview and Autism Diagnostic Observation Schedule administered by AGRE personnel. All subjects met criteria for autism according to the ADI-R and seventeen met criteria for autism and eight for ASD according to the ADOS. Five subjects with ASD were being treated with stimulants (2 methylphenidate, 2 dextroamphetamine); 1 was being treated with a selective norepinephrine reuptake inhibitor (atomoxetine); 1 was being treated with an anti-convulsant (levetiracetam); 2 were being treated with anti-depressants (1 fluoxetine, 1 fluvoxamine); and 1 was being treated with an anti-psychotic (risperidone). However, no controls were undergoing neuropharmacologic treatment at time of MRS. Control subjects were recruited from local community schools. Exclusion criteria for healthy controls included any lifetime significant medical or Axis I mental disorder based upon the KSADS or the Diagnostic Interview Schedule for Children (C-DISC-4, Shaffer et al., 2000) interview with the parent [96], with the following exceptions. As 4 of the ASD subjects were being treated with stimulant medications, we included one control subject meeting criteria for inattentive attention-deficit disorder (9 inattentive symptoms on the DISC-IV) and four subjects with 1–2 inattentive symptoms and 2–3 hyperactive symptoms as assessed by the DISC-IV in the control group. The samples did not differ significantly in age. Mean full-scale IQ, assessed using either the Weschler Intelligence Scale for Children (Weschler 1991) or the Weschler Adult Intelligence Scale or (WASI) (Wechsler Abbreviated Scale of Intelligence – WASI) [97], was 106.6±13.5 (76–142) for the sample with ASD and 101.2±13.6 (65–118) for the control sample. This was not a significant difference. One control subject had full-scale IQ 65 and therefore met a formal criterion for mental retardation. This was an otherwise normally functioning subject who did not qualify for any other psychiatric or developmental disorder. Exclusion of this subject did not change the study results. All other participants in both groups had full-scale IQ >75. The study was approved by the UCLA Human Subjects Review Board and we obtained written, informed consent from all subjects or from the subjects' parents or guardians.

MRI and multi-voxel ^{1}H MRSI were acquired contemporaneously at 1.5 T on a Siemens Sonata system with quadrature head coil. No subjects were sedated at time of scan. After initial

localizer, an axial-oblique whole-brain double turbo spin-echo (DTSE) structural MRI was acquired oriented parallel to the genu-splenium line as seen in the sagittal plane. This was followed by a sagittal T1-weighted high-resolution whole-brain SPGR structural MRI volume (TR/TE = 25/11 ms, NEX = 1, partition thickness = 1.2 mm contiguous, in-plane resolution = 1×1 mm^2). Water-suppressed ^{1}H MRSI (PRESS, TR/TE = 1500/30 ms, NEX = 8, slab thickness = 9 mm, in-plane resolution = 11×11 mm^2; Fig. 4) was acquired in the plane of the DTSE. The "PRESS box" – acquisition volume from which usable spectra could be obtained – measured 4×4 voxels in cross-section in every subject. The nominal voxel size was 9 mm ×11 mm ×11 mm ≈ 1.1 cc. Identical voxel positioning procedures were employed for subjects with ASD and controls by operators blinded to subject diagnosis. The pACC PRESS box straddled the longitudinal midline and was positioned with its posterior end at the rostrum of the corpus callosum, set just far back enough to prevent the anterior end of the box from contacting extracranial tissue. The slab was also centered dorsoventrally about the callosal rostrum. The lateral-mesial (left-right) position of the grid was moved to minimize differences in voxel composition. In particular, where subject anatomy permitted, the gridlines were positioned such that voxels lay entirely in left or entirely in right pACC and also such that gray-matter content of voxels generally was maximized. Thus, posterior voxels of this box sampled pACC and anterior voxels sampled mesial superior frontal cortex. Lateral voxels sampled prefrontal white matter. This PRESS scan was immediately followed by non-water-suppressed PRESS MRSI (NEX = 1, otherwise identical parameters). Finally, the whole-brain SPGR was repeated.

Operators were blinded to subject identity during MRI and MRSI post-processing. Offline, for each subject, the two whole-brain SPGR volumes were coregistered to each other and averaged together to enhance signal-to-noise ratio. The averaged SPGR was then manually edited to remove non-brain tissue. Automated programs were used to correct for magnetic field inhomogeneities [98], realign the images into a standard orientation using rigid-body transformations [99], and segment the volume into whole-brain masks representing gray matter, white matter, and CSF using a partial-volume correction method [100]. The masks were reverse-transformed to the subject's native space and binarized.

Siemens MRSI data were processed automatically with LCModel [81]. LCModel yielded absolute levels in Institutional Units (IU) scaled to water for the five major metabolite peaks. Numerous weaker resonances, in particular lipids and macromolecules, were included in the fit.

The UCLA MRSI Voxel Picker (MVP) version 1.0 software suite [101,102] was used for MRI/MRSI co-processing. The averaged SPGR volume and its gray-matter, white-matter, and CSF component masks were imported into MVP together with the MRSI raw data file and LCModel output. MVP reconstructed the subject's SPGR and displayed it in a guided user interface (GUI) in register with the corresponding MRSI PRESS volume in its plane-of-acquisition. MVP similarly reconstructed the whole-brain gray-matter, white-matter, and CSF binary masks; computed the volume% gray matter, white matter, and CSF in each MRSI voxel; and corrected the LCModel-derived levels of each metabolite for voxel CSF content. Metabolite levels were not corrected for T1- or T2-relaxation. Quality control of MRSI spectra was also implemented automatically by MVP, supplemented by operator inspection. Only spectra that showed a linewidth ≤0.1 ppm and a signal-to-noise ratio ≥3 were used for subsequent analysis. Furthermore, within each voxel, MVP

Table 3. Experiment 2: Subject group characteristics.

group	gender	age, years	full-scale IQ	medication
ASD	19 male, 7 female	10.2±3.3 (6.1–17.5)	106.6±13.5 (76–142)	5 stimulants, 1 anti-convulsant, 2 anti-depressants, 1 anti-psychotic
Typically developing	11 male, 5 female	11.8±3.0 (7.3–16.6)	101.2±13.6 (65–118)	none

values for age and IQ are group mean ± standard deviation (range).
doi:10.1371/journal.pone.0038786.t003

retained only those metabolite values that LCModel considered reliable (SD ≤20%). Voxels were selected by the operator on the MVP GUI in left and right hemispheres for pACC and for adjacent left and right prefrontal white matter. Within each structure, MVP averaged together the metabolite levels and tissue composition for all voxels that contained ≥50 vol% gray matter (≥70 vol% white matter for the white-matter regions), which satisfied the foregoing quality-control criteria.

Data were rank-transformed for non-parametric statistical analyses. MRSI voxel tissue composition (volume% gray matter, white matter, CSF) was compared between groups using independent T-test. To account for multiple comparisons, omnibus testing of CSF-corrected metabolite levels was performed prior to between-group regional comparisons. In particular, for each metabolite a repeated-measures ANCOVA (R-ANCOVA) was performed with Hemisphere (two levels: left, right) as within-subjects factor and Group (two levels: autism, control) as between-subjects factor. Tissue composition was included as covariate in the event of significant differences between groups. For metabolites for which R-ANCOVA yielded a significant main effect or interaction involving Group, post-hoc ANCOVA was performed comparing the between-group metabolite levels in each individual region, with volume% tissue composition included as covariate as appropriate.

As a further test of the possible influence of white-matter intrusion on pACC results, metabolite levels were compared between groups in adjacent left and right prefrontal white matter using independent T-test, to see if the same metabolite effects were present as in the cortex. Criterion for statistical significance for all tests was $p < 0.05$.

Results and Discussion

MRSI voxel tissue compositions are listed in Table 4. In both left ($p < 0.0005$) and right ($p < 0.01$) pACC volume% gray matter was significantly higher in subjects with ASD than in controls. Contrary to expectation, mean voxel volume% gray matter was 10–20% lower and mean voxel volume% white matter was 5–10% higher than the corresponding values in Experiment 1. The Experiment 1 strategem of varying MRS voxel dimensions was apparently more effective than using smaller MRSI voxels of a fixed size in maximizing gray-matter content. Based on these findings, volume% gray and volume% white matter were included as covariates in between-group comparisons of metabolite levels.

Fig. 4 shows a sample MRSI spectrum from left pACC. An appreciable Glx peak is visible next to the tNAA peak at 2.01 ppm. Table 4 lists group-mean CSF-corrected LCModel-derived metabolite values in left and right pACC. Omnibus R-ANCOVA for pACC covarying volume% left and right pACC gray matter and white matter indicated significant main effects of
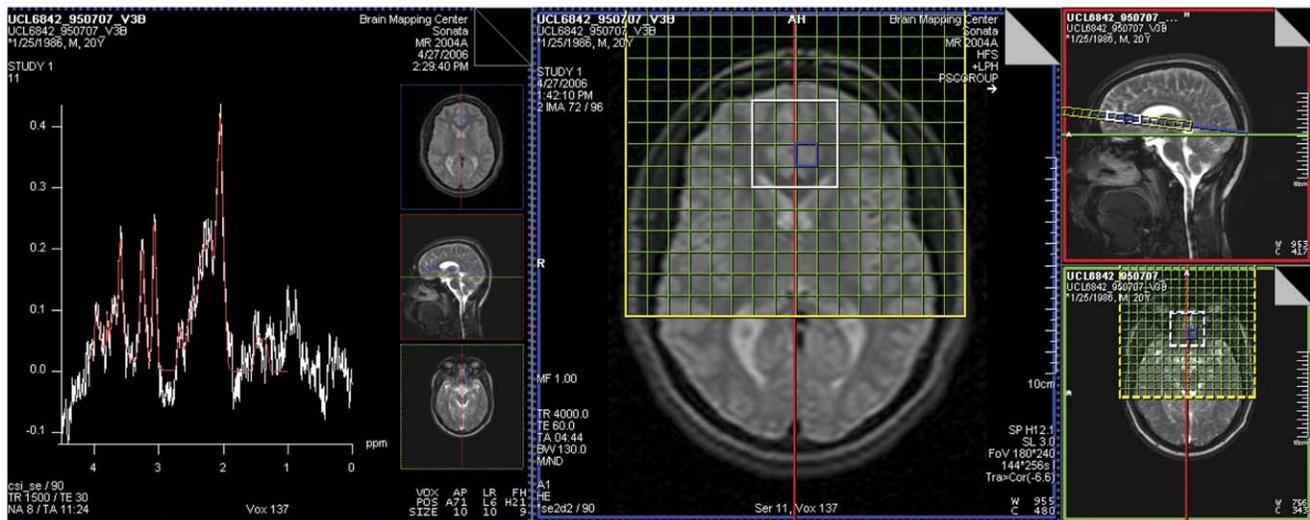
Figure 4. (*Right three panels*) MRI sections showing positioning of axial-oblique (parallel to genu-splenium line in sagittal plane) proton magnetic resonance spectroscopic imaging (¹H MRSI, TR/TE = 1500/30 ms) slab (*green grid*). The PRESS acquisition volume (*white box*) sampled bilateral pregenual anterior cingulate cortex (pACC, posterior mesial voxels), mesial superior frontal cortex (anterior mesial voxels) and laterally adjacent white matter (lateral voxels). (*Left panel*) sample spectrum from left pACC voxel selected in blue. The white trace depicts the raw data, the *red trace* is a summary fit provided by the Siemens Sonata software. This is superseded by a definitive fit provided by LCModel. An appreciable Glx peak is evident. Experiment 2.
doi:10.1371/journal.pone.0038786.g004

Table 4. Experiment 2: Voxel tissue content and proton magnetic resonance spectroscopic imaging (¹H MRSI) metabolite levels in bilateral pregenual anterior cingulate cortex (pACC) voxel.

	ASD		Healthy Control	
	mean ± SD	range	mean ± SD	range
Left pregenual Anterior Cingulate Cortex				
vol% GM	**77.7±3.8***	69.5–90.2	67.6±9.5	51.9–85.5
vol% WM	13.2±5.4	5.1–23.4	17.2±8.7	8.7–41.9
vol% CSF	9.1±5.6	1.6–19.1	8.6±6.7	0.6–21.2
tNAA	7.7±1.0	5.6–9.2	7.0±1.0	4.6–8.3
Glx	13.6±1.8	10.0–17.6	13.4±1.5	11.5–17.3
Cr	5.3±0.9	3.6–6.9	5.0±0.7	3.9–6.2
Cho	1.5±0.3	1.1–2.1	1.4±0.2	1.0–1.8
mI	4.2±0.7	2.8–5.5	3.9±0.8	2.4–5.2
Right pregenual Anterior Cingulate Cortex				
vol% GM	**75.9±3.5**	69.4–82.8	70.2±8.7	58.0–90.3
vol% WM	14.8±4.4	6.9–24.6	18.7±12.0	2.8–37.7
vol% CSF	8.9±3.8	2.8–16.9	10.4±7.1	0.7–22.1
tNAA	**7.6±1.0**	5.1–10.0	6.9±1.4	5.4–9.2
Glx	**14.5±2.2***	9.2–19.1	13.2±2.6	9.5–17.5
Cr	**5.4±0.9***	3.9–7.3	5.0±1.0	3.9–7.1
Cho	1.5±0.3	1.0–2.3	1.4±0.3	1.1–1.9
mI	4.1±0.7	2.7–5.5	3.9±1.1	2.9–6.6

*p<0.05 *vs.* controls ANCOVA following omnibus R-ANCOVA both covarying vol% GM and WM on rank-transformed (non-parametric) data. Abbreviations as in Table 2.

doi:10.1371/journal.pone.0038786.t004

Group for tNAA ($F_{(1,26)} = 5.4$, p<0.05) and Cr ($F_{(1,26)} = 7.2$, p<0.05) and a significant Group-by-Hemisphere interaction for Glx ($F_{(1,24)} = 4.6$, p<0.05). In post-hoc ANCOVA covarying volume% gray and white matter, in right pACC only, Glx (9.5%, $F_{(1,33)} = 4.9$, p<0.05), Cr (6.7%, $F_{(1,35)} = 6.5$, p<0.05), and tNAA (10.2%, $F_{(1,35)} = 8.2$, p<0.01) were significantly higher in the sample with ASD than in the control sample (Fig. 5). Glx was above the control mean for 16 of 23 subjects with ASD. Similar Glx elevation was observed when left and right pACC metabolite levels were averaged together. Upon removing subjects on medication, a notable Glx excess (8.5%) was still present in right pACC in the sample with ASD, though (perhaps due to the smaller number of subjects) this was no longer statistically significant. MRSI metabolite levels were also interrogated in left and right prefrontal white matter proximally lateral to the pACC in the same slab. In the sample with ASD, mean volume% white matter in these voxels was 86.3% ±4.6% (77.7–95.6%) on the left and 83.5% ±6.1% (74.3–96.2%) on the right; for the control sample, the values were 84.9% ±9.4% (70.0–99.5%) on the left and 79.9% ±5.6% (71.6–87.5%) on the right. There were no significant between-group differences in volume% white matter, gray matter, or CSF in these white-matter regions. In the sample with ASD, Glx in these voxels was 9.2±2.1 IU (6.0–13.5 IU) on the left and 9.7±1.4 IU (7.8–12.6 IU) on the right; for the control sample, the values were 9.5±0.9 IU (8.2–10.7 IU) on the left and 10.7±1.7 IU (8.5–13.2 IU) on the right. There were no significant between-group differences in Glx, Cr, tNAA or any other metabolite in these white-matter regions.
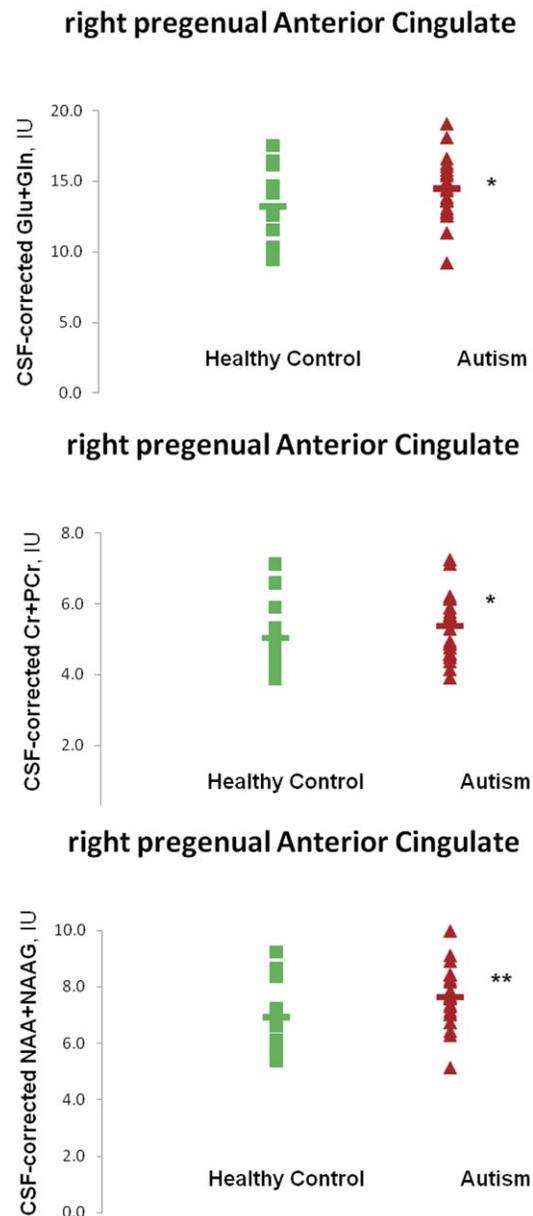
Figure 5. LCModel-derived absolute metabolite levels in Institutional Units (IU) corrected for voxel CSF-content for subjects with *ASD* (*red triangles*) **and healthy controls** (*green squares*) **in right pACC.** Horizontal bars denote group means. Values are shown for glutamate + glutamine ("Glx"; *top*), creatine + phosphocreatine (*middle*), and N-acetyl-aspartate + N-acetyl-aspartyl-glutamate. Note elevations of all three metabolites in subjects with *ASD*. *p<0.05, **p<0.01 (ANCOVA following R-ANCOVA of rank-transformed, therefore non-parametric data.) Experiment 2.
doi:10.1371/journal.pone.0038786.g005

This multi-voxel MRS investigation of glutamatergic metabolites in pACC yielded three major findings in the right pACC only: 1) Glx was higher in subjects with ASD than in typically-developing control subjects, 2) Cr was higher in subjects with ASD, and 3) tNAA was higher in subjects with ASD. These findings reinforce the notion from Experiment 1 that pACC metabolism is abnormal in ASD, with hyperglutamatergia as one feature. Abnormalities in Cr and tNAA metabolism are less

reliably supported. All three effects may be lateralized to the right pACC.

The first finding was elevated Glx in right pACC in ASD. As with the finding from Experiment 1 of elevated Glx in midline (left + right) pACC, this result supports hyperglutamatergic theories of ASD. All of the arguments advanced in the Discussion of Experiment 1 regarding the possible mechanisms and consequences of this hyperglutamatergia also apply here.

The second finding was elevated Cr in right pACC in ASD. As in the Discussion of the diminished Cr found in Experiment 1, this could be a sign of inefficient utilization of local cell energy, only with an aberration in the opposite direction in this instance.

The third finding was elevated tNAA in right pACC in ASD. An elevation in tNAA = NAA + NAAG may represent higher levels of NAA, of NAAG, or of both. Local elevations of NAA could result from multiple mechanisms, including faster astrocyte-membrane decomposition of NAAG into Glu and NAA [85], slower oligodendrocyte-membrane degradation of NAA into acetate and aspartate [103,104], slower intraneuronal synthesis of NAAG out of NAA and Glu [105], and/or faster intraneuronal NAA synthesis out of aspartate and acetyl-CoA [103,106]. Elevations of NAAG could result from faster pre-synaptic vesicular release [84], slower astrocytic decomposition into Glu and NAA, and faster neuronal synthesis out of NAA and Glu. Additionally, some genetic studies associate ASD with the SLC25A12 gene coding for the aspartate/glutamate carrier aralar1 in the mitochondrial membrane [19–23]. This carrier transports aspartate ions across the membrane out of the mitochondrion into the cytoplasm in exchange for Glu ions that leave the cytoplasm and enter the mitochondrion. Inside the mitochondrion, aspartate may be consumed by NAA synthesis and Glu may be consumed by the Krebs Cycle. Thus, any genetic variant that decreases transport efficiency and/or mitochondrial membrane density of aralar1 (if such be the case in ASD) could contribute to simultaneous elevation of Glx and tNAA, as seen in Experiment 2.

^{1}H MRS has linked glucose metabolic rate to tNAA [107] and to Glx [108], while ^{13}C MRS has linked glucose metabolic rate to NAA [109] and to Glu [110]. Among the factors underlying this linkage may be direct transport of water generated in energetic catabolism out of the neuron by NAA and NAAG [111,112] and/or regulation of neuronal and glial water content by osmolytic NAA and Glu [87]. Thus, elevations of all three metabolites (Glx, Cr, and tNAA) may be associated with disturbed brain energy metabolism in ASD. The lack of significant between-group differences in the levels of these three metabolites in proximal prefrontal white matter suggests that the effects are characteristic of local cortex and not white matter.

Each of the three metabolite elevations was apparent only in the right pACC. These findings join prior neuroimaging reports of lateralized effects of ASD within the anterior cingulated [42,53,60–62], specifically to right anterior cingulate (as reviewed by Mundy) [72] in some cases. It is possible that, with more subjects, effects might be observed in both cerebral hemispheres.

Some subjects with ASD but no controls were receiving psychotropic medication at time of scan. MRSI voxels contained significantly more gray matter in subjects with ASD than in controls, although voxel tissue composition was covaried for and results of a targeted sampling of high white-matter voxels appeared to rule-out the possibility that observed effects were due to between-group differences in voxel tissue content.

Discussion

The small pilot investigation, Experiment 1, indicated elevated Glx in pACC in ASD. A larger follow-up study, Experiment 2, in which the sample with ASD and the control sample were now better matched for gender and IQ again found elevated Glx in ASD, albeit restricted to right pACC. Thus, two separate studies using independent samples of children with ASD and controls and scanning on two different systems (GE, Siemens) both support the idea of pACC hyperglutamatergia in ASD.

As discussed in our review (Levitt et al., in press) [113], prior MRS studies reporting Glu or Glx in ASD have yielded mixed results, presumably due to differences in subject samples and MRS methods. Using rigorous MRSI methods, Friedman et al. (2003, 2006) [31,32] found no effects of ASD on Glx in the cingulate. Unfortunately, these authors do not specify which subregion(s) of the cingulate they sampled. Also, all the subjects with ASD in their study underwent propofol sedation at time of scan, whereas that was the case for only one subject in Experiment 1 and for none in Experiment 2. Shulman et al. (2003, 2009) point out that brain energetic metabolism, and thence the rate of Glu-Gln cycling and thereby possibly Glx levels, is intimately related to anesthesia-induced level of consciousness [114,115]. Finally, the subjects in Friedman et al. (2003, 2006) were considerably younger (<5 years old) than ours. Anatomic neuroimaging suggests differences between ASD in early and later childhood; for example, the well-known observation of brain overgrowth in ASD between 2–4 years [116,117] that arrests or normalizes in later childhood and adolescence [118,119]. Changes in regional neurometabolite levels in the developmental course of ASD may similarly underlie differences between our Glx findings and those of the Seattle Group. DeVito et al. (2007) [28] obtained below-normal Glx and tNAA diffusely in cortical gray matter in subjects with ASD. In particular, endpoint values were extrapolated from linear plots of metabolite levels sampled from voxels across entire cerebral lobes. Hence, it is not clear what levels of this metabolite were locally in pACC. Also, their TE of 135 ms leaves a rather small Glx signal that is perhaps less reliable than the signals of other metabolites. Sampling the amygdala-anterior hippocampus, Page et al. (2006) [47] measured elevated Glx in their sample with ASD. Experiments 1 and 2 are not strictly comparable with these prior studies as the latter did not specifically target the pACC using short-TE (25–30 ms) spectroscopy; to that extent, the present findings are novel. Using methods similar to our, Bernardi et al. (2011) [53] observed depressed Glx in right pACC, the opposite of the present findings, but in adult subjects with ASD. On the one hand, these opposite findings may reflect differences between adults and children. On the other hand, metabolite levels in our study are CSF-corrected and take account of MRSI voxel tissue composition while Bernardi et al. (2011) [53] do not provide this information. As metabolite levels vary between tissue types, it is possible that metabolite effects in Bernardi et al. (2011) [53] are confounded with intersubject variation in voxel tissue composition. Thus, while our studies of ASD offer anatomically highly targeted assays of pACC metabolite levels at short-TE accounting for voxel tissue composition, no previous study we are aware of offers comparable methodological rigor in the same age range (middle-childhood to adolescence).

Hence, we think that our two experiments add support to the notion that hyperglutamatergia exists at least in pACC and at least in middle to late childhood and adolescence in ASD. To determine whether this applies also in early childhood, a subsampling of the Seattle data within the pACC portion of their MRSI slab might be helpful; a more stringent and more

challenging test would be to acquire from the region in non-anesthetized children, perhaps while sleeping or using very rapid pulse sequences. To determine whether hypo- or hyperglutama-tergia applies in pACC in adults with ASD, results of an analysis of the Bernardi et al. (2011) data taking account of voxel tissue composition might be helpful.

The findings of hyperglutamatergia in our studies are generally consistent with recent broader theories of autistic spectrum disorders that emphasize an imbalance in cortical excitation vs. inhibition [120,121]. Elevated glutamatergic metabolism, as seen in the present results, may be a consequence of deficient central GABAergic inhibition, as proposed in these theories. Based on human post-mortem and genetic and rodent ASD model investigations, inadequate GABAergic inhibition may have multiple developmental causes including underexpression of the GAD65 and GAD67 enzymes (that synthesize GABA from Glu), atypical GABA$_A$ receptor subunit composition, and failure of neuroligin and neurexin synaptic binding proteins to appose post-synaptic GABA receptors precisely to presynaptic release sites. In the past few years, translational neuroscience has been making a mounting case for hypofunctioning of brain GABAergic systems ASD that could lead to excess brain glutamatergic metabolism.

Whereas Experiment 1 found diminished pACC Cr in the sample with ASD, Experiment 2 found elevated Cr in right pACC. Thus, abnormal Cr in pACC in ASD, if it does exist, is more variable and harder to reproduce than abnormal Glx. This variability might reflect unstable local cell energetics that induce an expanded creatine-phosphocreatine ATP buffer in some subjects and a contracted buffer in others. Page et al. (2006) [47] also observed elevated Cr in amygdala-hippocampus in ASD, and Levitt et al. (2003) [42] observed effects of ASD diagnosis on Cr in occipital cortex and caudate, so there is precedence for abnormal Cr in ASD, albeit in other brain regions.

Elevated tNAA was found in pACC in ASD in Experiment 2 only. Again, abnormal tNAA in ASD may be harder to reproduce than elevated Glx. In prior work, Oner et al. (2007) [46] registered higher tNAA/Cr and tNAA/Cho in right anterior cingulate cortex in subjects with Asperger's syndrome than in controls and Fujii et al. (2010) [33] found lower tNAA/Cr in anterior cingulate in subjects with autism than in controls. Interpretation of these results is partially obscured by normalization to Cr, which itself may vary, but they do suggest heterogeneous effects of ASD on tNAA. In other brain regions (reviewed in Levitt et al, in press) [113], investigators have often found below-normal tNAA or its ratios in ASD, although findings of above-normal and no difference also exist. How plausible is a local elevation of tNAA in the pACC? In addition to the above-cited MRS results, data from recent fMRI and hybrid fMRI-MRS experiments do, in fact, strongly suggest a special role for the pACC in ASD and autistic symptomatology. The pACC, for example, was one of the few brain regions demonstrating significant effects of ASD diagnosis in a recent metaanalysis of fMRI studies [66]. Working in healthy subjects, the same researchers related fMRI functional connectivity with the pACC with elevated levels of autistic traits [65]. Also in healthy

controls, Duncan et al. (2011) [76] found correlations localized to pACC between MRS Glx and an fMRI effect related to subject empathy, low empathy being a common symptom of ASD. Finally, elevated intensity was observed in at-risk carriers of an autism-associated CNTNAP2 allele in pACC [75]. These and other neuroimaging results give ample evidence for focal effects of ASD diagnosis and autistic traits and autistic symptoms in the pACC. It is therefore not surprising to find MRS metabolic effects particular to that brain region.

Experiment 2 alleviated several but not all limitations of Experiment 1. Both studies were still conducted at low-field (1.5 T) and expressed their results as Glx rather than as Glu and Gln separately. Based on low field strength and, in the case of MRSI, small voxel size, our quality control procedures used the standard 20% SD criterion of the LCModel fitting package and a SNR cut-off of 3 for MRSI and 5 for single-voxel MRS. Although some spectroscopists might prefer stricter cut-offs, working with these values we found that individual metabolite peaks were typically readily identified by eye and easily fit by automated routines. Also single-subject data quality was frequently higher than the cut-off values. In neither study was it possible to match between-group voxel tissue-composition thoroughly (although differences were dealt with through statistical covariates and co-sampling proximal white matter). Efforts to match tissue composition may have been aggravated by putative effects of ASD on anterior cingulate cortical volume or thickness [58–61]. Future MRS and MRSI studies at 3 T will allow smaller, hopefully more tissue-pure voxels and also better spectral segregation of Glu and Gln. Regarding the latter, better segregation might also be achieved by acquiring spectra at TE = 80 ms, thought to be optimal for quantifying Glu [122–124]. Future investigations should also include MR relaxation studies, as autism may affect metabolite and water relaxation times [31,125]. Finally, in both Experiments, several subjects with ASD were undergoing treatment with psychotropic medication at time of scan. Ideally, one would test only drug-naïve subjects, although, given clinical realities, this can be difficult to achieve on a practical time scale. These limitations notwithstanding, the present findings suggest that Glx is elevated locally in pregenual anterior cingulate cortex in subjects with ASD. This elevation, combined with less certain effects of autism on Cr and tNAA may reflect disturbances of cell-energy metabolism.

Acknowledgments

Author Contributions

Conceived and designed the experiments: JON JGL JRA. Performed the experiments: JON AJF JRA. Analyzed the data: AB JON JAK AJF VWY RL CK JGL. Contributed reagents/materials/analysis tools: JON JTM AWT. Wrote the paper: AB JON JGL JTM. Designed the software used in analysis: JON AJF JRA. Radiologic review of MRIS: NS. Subject recruitment: JGL.

References

1. Carlsson ML (1998) Hypothesis: Is infantile autism a hypoglutamatergic disorder? Relevance of glutamate-srotonin interactions for pharmacotherapy. J Neural Transm 105: 525–535.
2. Fatemi SH (2008) The hyperglutamatergic hypothesis of autism. Prog Neuro-Psychopharm Biol Psychiatry 32: 911.
3. Jamain S, Betancur C, Quach H, Philippe A, Fellous M, et al. (2002) Linkage and association of the glutamate receptor 6 gene with autism. Molecular Psychiatry 7: 302–310.
4. Polleux F, Lauder JM (2004) Toward a developmental neurobiology of autism. Ment Retard Devel Disabilities Res Rev 10: 303–317.
5. McDougle CJ, Erickson CA, Stigler KA, Posey DJ (2005) Neurochemistry in the pathology of autism. J Clin Psychiatry 66(Suppl 10):: 9—18.
6. Pardo CA, Eberhart CG (2007) The neurobiology of autism. Brain Pathol 17: 434–447.
7. Rubenstein JL, Merzenich MM (2003) Model of autism: Increased ratio of excitation/inhibition in key neural systems. Genes Brain Behav 2: 255–267.
8. Ballaban-Gil K, Tuchman R (2000) Epilepsy and epileptiform EEG: Association with autism and language disorders. Ment Retard Disability Res Rev 6: 300–308.

9. Aldred S, Moore KM, Fitzgerald M, Waring RH (2003) Plasma amino acid levels in children with autism and their families. J Autism Devel Disord 33(1): 93–97.

10. Moreno H, Borjas L, Arrieta A, Saez L, Prassad A, et al. (1992) Heterogeneidad clínica del síndrome autista: Un estudio en sesenta familias. Investigación Clínica 33(1): 13–31.

11. Moreno-Fuenmayor H, Borjas L, Arrieta A, Valera V, Socorro-Candanoza L (1996) Plasma excitatory amino acids in autism. Investigación Clínica 37(2): 113–128.

12. Rolf LDH, Grotemeyer KH, Haarman FY, Kehren H (1993) Serotonin and amino acid content in platelets of autistic children. Acta Psychiatrica Scand 87: 312–316.

13. Shinohe A, Hashimoto K, Nakamura K, Tsujii M, Iwata Y, et al. (2006) Increased serum levels of glutamate in adult patients with autism. Prog Neuro-Psychopharmacol Biol Psychiatry 30: 1472–1477.

14. Purcell AE, Jeon OH, Zimmerman AW, Blue ME, Pevsner JP (2001) Postmortem brain abnormalities of the glutamate neurotransmitter system in autism. Neurology 57: 1618–1628.

15. Brune CW, Kim S-J, Hanna GL, Courchesne E, Lord C, et al. (2008) Family-Based Association Testing of OCD-Associated SNPs of SLC1A1 in an Autism Sample. Autism Res 1(2): 108–113.

16. Serajee FJ, Zhong H, Nabi R, Huq AH (2003) The metabotropic glutamate receptor 8 gene at 7q31: Partial duplication and possible association with autism. J Med Gen 40(4): e42.

17. Dutta S, Das S, Guhathakurta S, Sen B, Sinha S, et al. (2007) Glutamate Receptor 6 gene (GluR6 or GRIK2) polymorphisms in the Indian population: A genetic association study on autism spectrum disorder. Cell Mol Neurobiol 27: 1035–1047.

18. Buttenschon HN, Lauritsen MB, El Daoud A, Hollegaard M, Jorgensen M, et al. (2009) A population-based association study of glutamate decarboxylase as a candidate gene for autism. J Neural Transm 116: 381–388.

19. Palmieri L, Papaleo V, Porcelli V, Scarcia P, Gaita L, et al. (2008) Altered calcium homeostasis in autism-spectrum disorders: evidence from biochemical and genetic studies of the mitochondrial aspartate/glutamate carrier AGC1. Molecular Psychiatry 15(1): 38–52.

20. Ramoz N, Reichert JG, Smith CJ, Silverman JM, Bespalova IN, et al. (2004) Linkage and association of the mitochondrial aspartate/glutamte carrier SLC25A12 gene with autism. Am J Psychiatry 161: 662–669.

21. Seguardo R, Conroy J, Meally E (2005) Confirmation of association between autism and the mitochondrial aspartate/glutamate carrier SLC25A12 gene on chromosome 2q31. Am J Psychiatry 162: 2182–2184.

22. Silverman JM, Buxbaum JD, Ramoz N, Schmeidler J, Reichenberg A, et al. (2007) Autism-related routines and rituals associated with a mitochondrial aspartate/glutamate carrier SLC25A12 polymorphism. Am J Med Gen Part B: Neuropsychiatric Gen 147(3): 408–410.

23. Turunen JA, Rehnström K, Kilpinen H, Kuokkanen M, Kempas E, et al. (2008) Mitochondrial aspartate/glutamate carrier SLC25A12 gene is associated with autism. Autism Res 1: 189–192.

24. Blasi F, Bacchelli E, Carone S, Toma C, Monaco AP, et al. (2006) SLC25A12 and CMYA3 gene variants are not associated with autism in the IMGSAC multiplex family sample. Eur J Hum Gen 14: 123–126.

25. Correia C, Coutinho AM, Diogo L, Grazina M, Marques C, et al. (2006) High frequency of biochemical markers for mitochondrial dysfunction in autism: No association with the mitochondrial aspartate/glutamate carrier SLC25A12 gene. J Autism Dev Disord 36: 1137–1140.

26. Rabionet R, McCauley JL, Jaworski JM, Ashley-Koch AE, Martin ER, et al. (2006) Lack of association between autism and SLC25A12. Am J Psychiatry 163: 929–931.

27. Lepagnol-Bestel A-M, Maussion G, Boda B, Cardona A, Iwayama Y, et al. (2008) SLC25A12 expression is associated with neurite outgrowth and is upregulated in the prefrontal cortex of autistic subjects. Molec Psychiatry 13: 385–397.

28. DeVito TJ, Drost DJ, Neufeld RW, Rajakumar N, Pavlosky W, et al. (2007) Evidence for Cortical Dysfunction in Autism: A Proton Magnetic Resonance Spectroscopic Imaging Study. Biol Psychiatry 61: 465–473.

29. Endo T, Shioiri T, Kitamura H, Kimura T, Endo S, et al. (2007) Altered chemical metabolites in the amygdala-hippocampus region contribute to autistic symptoms of autism spectrum disorders. Biol Psychiatry 62: 1030–1037.

30. Fayed N, Modrego P (2005) Comparative study of cerebral white matter in autism and attention-deficit/Hyperactivity disorder by means of magnetic resonance spectroscopy. Acad Radiol 12: 566–569.

31. Friedman SD, Shaw DW, Artru AA, Richards TL, Gardner J, et al. (2003) Regional brain chemical alterations in young children with autism spectrum disorder. Neurology 60(1): 100–107.

32. Friedman SD, Shaw DW, Artru AA, Dawson G, Petropoulos H, et al. (2006) Gray and white matter brain chemistry in young children with autism. Arch Gen Psychiatry 63: 786–794.

33. Fujii E, Mori K, Miyazaki M, Hashimoto T, Harada M, et al. (2010) Function of the frontal lobe in autistic individuals: a proton magnetic resonance spectroscopic study. J Med Invest 57: 35–44.

34. Gabis L, Huang W, Azizian A, DeVincent C, Tudorica A, et al. (2008) ^{1}H-Magnetic resonance spectroscopy markers of cognitive and language ability in clinical subtypes of autism spectrum disorders. J Child Neurol 23: 766–774.

35. Harada M, Taki MM, Nose A, Kubo H, Mori K, et al. (2011) Non-invasive evaluation of the GABAergic/glutamatergic system in autistic patients observed by MEGA-editing proton MR spectroscopy using a clinical 3 Tesla instrument. J Autism Dev Disord 41(4): 447–454.

36. Hardan AY, Minshew NJ, Melhem NM, Srihara S, Jo B, et al. (2008) An MRI and proton spectroscopy study of the thalamus in children with autism. Psychiatry Res: Neuroimaging 163: 97–105.

37. Hashimoto T, Kawano N, Fukuda K, Endo S, Mori K, et al. (1998) Proton magnetic resonance spectroscopy of the brain in three cases of Rett syndrome: comparison with autism and normal controls. Acta Neurol Scand 98: 8–14.

38. Hashimoto T, Tayama M, Miyazaki M, Yoneda Y, Yoshimoto T, et al. (1997) Differences in brain metabolites between patients with autism and mental retardation as detected by in vivo localized proton magnetic resonance spectroscopy. J Child Neurol 12: 91–96.

39. Hisaoka S, Harada M, Nishitani H, Mori K (2001) Regional magnetic resonance spectroscopy of the brain in autistic individuals. Neuroradiol 43: 496–498.

40. Kleinhaus NM, Richards T, Weaver KE, Liang O, Dawson G, et al. (2009) Biochemical correlates of clinical impairment in high-functioning autism and Asperger's disorder. J Autism Dev Disord 39: 1079–1086.

41. Kleinhaus NM, Schweinsburg BC, Cohen DN, Müller R-A, Courchesne E (2007) N-acetyl aspartate in autism spectrum disorders: Regional effects and relationship to fMRI activation. Brain Res 1162: 85–97.

42. Levitt JG, O'Neill J, Blanton RE, Smalley S, Fadale D, et al. (2003) Proton magnetic resonance spectroscopic imaging of the brain in childhood autism. Biol Psychiatry 54(12): 1355–1366.

43. Minshew NJ, Goldstein G, Dombrowski SM, Panchalingam K, Pettegrew JW (1993) A preliminary ^{31}P MRS study of autism: evidence for undersynthesis and increased degradation of brain membranes. Biol Psychiatry 33: 762–763.

44. Mori K, Hashimoto T, Harada M, Yoneda Y, Shimakawa S, et al. (2001) Proton magnetic resonance spectroscopy of the autistic brain. No To Hattatsu 33(4): 329–335.

45. Murphy DGM, Critchley HD, Schmitz N, McAlonan G, van Amelsvoort T, et al. (2002) Asperger syndrome: A proton magnetic resonance spectroscopy study of brain. Arch Gen Psychiatry 59: 885–891.

46. Oner O, Devrimci-Ozguven H, Oktem F, Yagmurlu B, Baskak B, et al. (2007) Proton MR spectroscopy: Higher right anterior cingulate N-acetylaspartate/choline ratio in Asperger syndrome compared with healthy controls. AJNR 28: 1494–1498.

47. Page LA, Daly E, Schmitz N, Simmons A, Toal F, et al. (2006) In vivo ^{1}H-magnetic resonance spectroscopy study of amygdala-hippocampal and parietal regions in autism. Am J Psychiatry 163: 2189–2192.

48. Perich-Alsina J, Aduna de Paz M, Valls A, Muñoz-Yunta JA (2002) Espectroscopía talámica por resonancia magnética en el autismo. Rev Neurol 34: S68–71.

49. Sokol DK, Dunn DW, Edwards-Brown M, Feinberg J (2002) Hydrogen proton magnetic resonance spectroscopy in autism: preliminary evidence of elevated choline/creatine ratio. J Child Neurol 17: 245–249.

50. Strauss WL, Unis AS, Cowan C, Dawson G, Dager SR (2002) Fluorine magnetic resonance spectroscopy measurement of brain fluvoxamine and fluoxetine in pediatric patients treated for pervasive developmental disorders. Am J Psychiatry 159: 755–760.

51. Suzuki K, Nishimura K, Sugihara G, Nakamura K, Tsuchiya KJ, et al. (2010) Metabolite alterations in the hippocampus of high-functioning adult subjects with autism. Int J Neuropsychopharmacol 13: 529–534.

52. Zeegers M, van der Grond J, van Daalen E, Buitelaar J, van Engeland H (2007) Proton magnetic resonance spectroscopy in developmentally delayed young boys with or without autism. J Neural Transm 114: 289–295.

53. Bernardi S, Anagnostou E, Shen J, Kolevzon A, Buxbaum JD, et al. (2011) In vivo ^{1}H-magnetic resonance spectroscopy study of the attentional networks in autism. Brain Research 1380: 198–205.

54. Casanova MF, Buxhoeveden DP, Switala AE, Roy E (2002) Minicolumnar pathology in autism. Neurology 58: 428–432.

55. Oblak AL, Gibbs TT, Blatt GJ (2010) Decreased GABA$_B$ receptors in the cingulate cortex and fusiform gyrus in autism. J Neurochem 114: 1414–1423.

56. Oblak AL, Gibbs TT, Blatt GJ (2010) Decreased GABA$_B$ receptors and benzodiazepine binding sites in the anterior cingulate cortex in autism. Autism Res 2: 205–219.

57. Simms ML, Kemper TL, Timbie CM, Bauman ML, Blatt GJ (2009) The anterior cingulate cortex in autism: heterogeneity of qualitative and quantitative cytoarchitectonic features suggests possible subgroups. Acta Neuropathol 118: 673–684.

58. Bonilha L, Cendes F, Rorden C, Eckert M, Dalgalarrondo P, et al. (2008) Gray and white matter imbalance – Typical structural abnormality underlying classic autism? Brain & Devel 30: 396–401.

59. Hyde KL, Samson F, Evans AC, Mottron L (2010) Neuroanatomical differences in brain areas implicated in perceptual and other core features of autism revealed by cortical thickness analysis and voxel-based morphometry. Human Brain Mapping 31: 556–566.

60. Jiao Y, Chen R, Ke X, Chu K, Lu Z, et al. (2010) Predictive models of autism spectrum disorder based on brain regional cortical thickness. NeuroImage 50: 589–599.

61. Ke X, Hong S, Tang T, Zou B, Li H, et al. (2008) Voxel-based morphometry study on brain structure in children with high-functioning autism. NeuroReport 19: 921–925.

62. Korkmaz B, Benbir G, Demirbilek V (2006) Migration abnormality in the left cingulate gyrus presenting with autistic disorder. J Child Neurol 21: 600.

63. Agam Y, Joseph RM, Berton JJS, Manoach DS (2010) Reduced cognitive control of response inhibition by the anterior cingulate cortex in autism spectrum disorders. NeuroImage 52: 336–347.

64. Dichter GS, Felder JN, Bodfish JW (2009) Autism is characterized by dorsal anterior cingulate hyperactivation during social target detection. SCAN 4: 215–226.

65. Di Martino A, Shehzad Z, Roy AK, Gee DG, Uddin LQ, et al. (2009b) Relationship between cingulo-insular functional connectivity and autistic traits in neurotypical adults. Am J Psychiatry 166: 891–899.

66. Di Martino A, Ross K, Uddin LQ, Sklar AB, Castellanos FX, et al. (2009a) Functional brain correlates of social and nonsocial processes in autism spectrum disorders: An activation likelihood estimation meta-analysis. Biol Psychiatry 65: 63–74.

67. Thakkar KN, Polli FE, Joseph JM, Tuch DS, Hadjikhani N, et al. (2008) Response monitoring, repetitive behaviour and anterior cingulate abnormalities in autism spectrum disorders (ASD). Brain 131: 2464–2478.

68. Nakamura K, Sekine Y, Ouchi Y, Tsujii M, Yoshikawa E, et al. (2010) Brain serotonin and dopamine transporter bindings in adults with high-functioning autism. Arch Gen Psychiatry 67(1): 59–68.

69. Siegel BV, Nuechterlein KH, Abel L, Wu JC, Buchsbaum MS (1995) Glucose metabolic correlates of continuous performance test performance in adults with a history of infantile autism, schizophrenics, and controls. Schiz Res 17: 85–84.

70. Murphy DGM, Daly E, Schmitz N, Toal F, Murphy K, et al. (2006) Cortical serotonin 5-HT2A receptor binding and social communication in adults with Asperger's syndrome: An in vivo SPECT study. Am J Psychiatry 163: 934–936.

71. Vlamings PHJM, Jonkman LM, Hoeksma MR, van Engeland H, Kemner C (2008) Reduced error monitoring in children with autism spectrum disorder: an ERP study. Eur J Neurosci 28: 399–406.

72. Mundy P (2003) Annotation: The neural basis of social impairments in autism: the role of the dorsal medial-frontal cortex and anterior cingulate system. J Child Psychol Psychiatry 44(6): 793–809.

73. O'Neill J, Sobel T, Vogt BA (2009) Localizing cingulate subregions of interest – SOIs – in magnetic resonance images guided by cytological parcellations. In: Vogt BA, editor. Cingulate Neurobiology & Disease. New York: Oxford University Press.

74. Vogt BA (2009) Regions and subregions of the cingulate gyrus. In: Vogt BA, editor. Cingulate Neurobiology and Disease. New York: Oxford University Press, 3–30.

75. Scott-Van Zeeland A, Abrahams BS, Alvarez-Retuerto AL, Sonnenblick LI, Rudie JD, et al. (2010) Altered functional connectivity in frontal lobe circuits is associated with variation in the autism risk gene CNTNAP2. Sci Transl Med 2: 56–80.

76. Duncan NW, Enzi B, Wiebking C, Northoff G (2011) Involvement of glutamate in rest-stimulus interaction between perigenual and supragenual anterior cingulate cortex: A combined fMRI-MRS study. Human Brain Mapping 32: 2172–2182.

77. Lord C, Rutter M, Le Couteur A (1994) Autism diagnostic interview-revised: a revised version of a diagnostic interview for caregivers of individuals with possible pervasive developmental disorders. J Autism Devel Disord 24(5): 659–685.

78. Lord C, Rutter M, DiLavore P, Risis S (1999) Autism Diagnostic Observation Schedule-WPS (WPS Edition). Los Angeles: Western Psychological Services.

79. Kaufman J, Birmaher B, Brent D, Rao U, Flynn C, et al. (1997) Schedule for Affective Disorders and Schizophrenia for School-Age Children-Present and Lifetime Version (K-SADS-PL): initial reliability and validity data. JAACAP 36(7): 980–988.

80. Wechsler D (1991) Wechsler Intelligence Scale for Children 3rd ed. New York: Psychological Corporation.

81. Provencher SW (2001) Automatic quantitation of localized in vivo ^{1}H spectra with LCModel. NMR Biomed 14: 260–264.

82. Blanton RE, Levitt JG, Thompson PM, Narr KL, Capetillo-Cunliffe L, et al. (2001) Mapping cortical asymmetry and complexity patterns in normal children. Psychiatry Res: Neuroimaging 107: 29–43.

83. Ross BD (1991) Biochemical considerations in ^{1}H spectroscopy. Glutamate and glutamine; myo-inositol and related metabolites. NMR Biomed 4: 59–63.

84. Williamson LC, Neale JH (1988) Calcium-dependent release of N-acetylaspartylglutamate from retinal neurons upon depolarization. Brain Res 475: 151–155.

85. Cassidy M, Neale JH (1993) N-acetylaspartylglutamate catabolism is achieved by an enzyme on the cell surface of neurons and glia. Neuropeptides 24: 271–278.

86. Petroff OAC, Mattson RH, Rothman DL (2000) Proton MRS: GABA and glutamate. Adv Neurol 83: 261–271.

87. Ross BD, Blüml S (2001) Magnetic resonance spectroscopy of the human brain. The Anat Record (New Anat) 265: 54–84.

88. Chaudhry FA, Reimer RJ, Krizaj D, Barber D, Storm-Mathisen J, et al. (1999) Molecular analysis of system N suggests novel physiological roles in nitrogen metabolism and synaptic transmission. Cell 99: 769–780.

89. Varoqui H, Zhu H, Yao D, Ming H, Erickson JD (2000) Cloning and functional identification of a neuronal glutamine transporter. J Biol Chem 275(6): 4049–4054.

90. Hertz L, Zielke HR (2004) Astrocytic control of glutamatergic activity: astrocytes as stars of the show. Trends Neurosci 27(12): 735–743.

91. Danbolt NC (2001) Glutamate uptake. Prog Neurobiol 65: 1–105.

92. Erecinska M, Silver IA (1989) ATP and Brain Function. J Cereb Blood Flow Metab 9: 2–19.

93. Siesjö BK (1978) Brain Energy Metabolism. Chichester: Wiley.

94. Walker JB (1979) Creatine: Biosynthesis, Regulation and Function. Advances in Enzymology. John Wiley: New York.

95. Rumsey JM, Ernst M (2000) Functional neuroimaging of autistic disorders. Ment Retard Devel Disabilities Res Rev 6: 171–179.

96. Shaffer D, Fisher P, Lucas CP, Dulcan MK, Schwab-Stone ME (2000) NIMH Diagnostic Interview Schedule for Children Version IV (NIMH DISC-IV): description, differences from previous versions, and reliability of some common diagnoses. J Am Acad Child Adolesc Psych 39(1): 28–38.

97. Wechsler D (1999) Wechsler Abbreviated Scale of Intelligence (WASI). Psychological Corporation, San Antonio.

98. Sled JG, Pike GB (1998) Standing-wave and rf penetration artifacts caused by elliptic geometry: an electrodynamic analysis of MRI. IEEE Trans Med Imaging 17: 653–662.

99. Woods RP, Grafton ST, Watson JD, Sicotte NL, Mazziotta JC (1998) Automated image registration: II. Intersubject validation of linear and nonlinear models. J Comput Assist Tomogr 22: 153–165.

100. Shattuck DW, Sandor-Leahy SR, Schaper KA, Rottenberg DA, Leahy RM (2001) Magnetic resonance image tissue classification using a partial volume model. NeuroImage 13: 856–876.

101. O'Neill J, Tseng PB, Pagare R, Frew AJ, Tafazoli S, et al. (2006) MRSI voxel picker (MVP): Software for co-evaluation of structural and spectroscopic information. ISMRM Workshop on Quantitative Spectroscopy. Warrenton, VA.

102. Seese RR, O'Neill J, Hudkins M, Siddarth P, Levitt J, et al. (2011) Proton magnetic resonance spectroscopy and thought disorder in childhood schizophrenia. Schiz Res 133:82–90.

103. Baslow MH (1997) A review of phylogenetic and metabolic relationships between the acylamino acids, N-acetyl-L-aspartic acid and N-acetyl-L-histidine in the vertebrate nervous system. J Neurochem 68(4): 1335–44.

104. Baslow MH (2000) Functions of N-acetyl-L-aspartate and N-acetyl-L-aspartylglutamate in the vertebrate brain: role in glial cell-specific signaling. J Neurochem 75(2): 453–459.

105. Cangro CB, Namboodiri MAA, Sklar LA, Corigliano-Murphy A, Neale JH (1987) Immunohistochemistry and biosynthesis of N-acetylaspartylglutamate in spinal sensory ganglia. J Neurochem 49: 1579–1588.

106. Patel TB, Clark JB (1979) Synthesis of N-acetyl-L-aspartate by rat mitochondria and its involvement in mitochondria/cytosolic carbon transport. Biochem J 184: 163–168.

107. O'Neill J, Eberling JL, Schuff N, Jagust WJ, Reed B, et al. (2000) Correlation of ^{1}H MRSI and ^{18}FDG-PET. Magn Reson Med 43: 244–50.

108. Pfund Z, Chugani DC, Juhasz C, Muzik O, Chugani HT, et al. (2000) Evidence for coupling between glucose metabolism and glutamate cycling using FDG PET and ^{1}H magnetic resonance spectroscopy in patients with epilepsy. J Cereb Blood Flow Metab 20(5): 871–878.

109. Moreno A, Ross BD, Bluml S (2001) Direct determination of the N-acetyl-L-aspartate synthesis rate in the human brain by (13)C MRS and [1-(13)C] glucose infusion. J Neurochem 77(1): 347–50.

110. Sibson NR, Shen J, Mason GF, Rothman DI, Behar KI, et al. (1998) Functional energy metabolism: in vivo ^{13}C-NMR spectroscopy evidence for coupling of cerebral glucose consumption and glutamatergic neuronal activity. Devel Neurosci 20(4–5): 321–330.

111. Baslow MH (2003) Evidence supporting a role for N-acetyl-L-aspartate as a molecular water pump in myelinated neurons in the central nervous system. An analytical review. Neurochem Int 40(4): 295–300.

112. Baslow MH, Dyakin VV, Nowak KL, Hungund BL, Guilfoyle DN (2005) 2-PMPA, a NAAG peptidase inhibitor, attenuates magnetic resonance signals in brain of anesthesized mice. J Molec Neurosci 26: 1–15.

113. Levitt JG, O'Neill J, Alger JR (in press) Magnetic resonance spectroscopy studies of autistic spectrum disorders (ASD). In: Blüml S, Panigrahy A (eds.) MR Spectroscopy of Pediatric Brain Disorders. Springer, NY.

114. Shulman RG, Hyder F, Rothman DL (2003) Métabolisme cérébral et conscience. CR Biologies 326: 253–273.

115. Shulman RG, Hyder F, Rothman DL (2009) Baseline brain energy supports the state of consciousness. PNAS 106(27): 11096–11101.

116. Schumann CM, Bloss CS, Barnes CC, Wideman GM, Carper RA, et al. (2010) Longitudinal magnetic renonance imaging study of corical development through early childhood in autism. J Neurosci 30:4419–27.

117. Sparks BF, Friedman SD, Shaw DW, Aylward EH, Echelard D, et al. (2002) Brain structural abnormalities in young children with autism spectrum disorder. Neurology 2002: 59:184–92.

118. Aylward EH, Minshew NJ, Field K, Sparks BF, Singh N (2002) Effects of age on brain volume and head circumference in autism. Neurology 59(2): 175–83.

119. Redcay E, Courchesne E (2005) When is the brain enlarged in autism? A meta-analysis of all brain size reports. Biol Psychiatry 58(1): 1–9.

120. Gogolla N, Leblanc JJ, Quast KB, Südhof TC, Fagiolini M, et al. (2009) Common circuit defect of excitatory-inhibitory balance in mouse models of autism. J Neurodev Disord 1(2): 172–181.

121. Pizzarelli R, Cherubini E (2011) Alterations of GABAergic signaling in autism spectrum disorders. Neural Plast 2011: p. 297153.

122. Hancu I, Frye M, Port J (2009) The case of the missing glutamine. ISMRM 17th Scientific Meeting and Exhibition, Honolulu, April 18–24.

123. O'Gorman RL, Noble J, Stone JM, Lythgoe DJ, McLean MA, et al. (2009) Reliability of in vivo glutamate detection with MRS at 3T. ISMRM 17th Scientific Meeting and Exhibition, Honolulu, April 18–24.

124. Schubert F, Gallinat J, Seifert F, Rinneberg H (2004) Glutamate concentrations in human brain using single voxel proton magnetic resonance spectroscopy at 3 Tesla. NeuroImage 21: 1762–1771.

125. Petropoulos H, Friedman SD, Shaw DWW, Artru AA, Dawson G, et al. (2006) Gray matter abnormalities in autism spectrum disorder revealed by T2 relaxation. Neurology 67: 632–636.